VOL. 2, NO. 11, November 2012 ISSN 2222-9833

ARPN Journal of Systems and Software

http://www.scientific-journals.org

Carrier-phase GNSS Attitude Determination and Control System for Unmanned Aerial Vehicle Applications

[1]Roberto Sabatini, Leopoldo Rodríguez, Anish Kaharkar, Celia Bartel, Tesheen Shaid
Cranfield University – Department of Aerospace Engineering, Cranfield, Bedford MK43 0AL, UK
[1]Corresponding author: r.sabatini@cranfield.ac.uk, phone +44 (0)1234 758290, www.cranfield.ac.uk

ABSTRACT

This paper presents the results of a research activity performed by Cranfield University to assess the potential of carrier-phase Global Navigation Satellite Systems (GNSS) for attitude determination and control of small to medium size Unmanned Aerial Vehicles (UAV). Both deterministic and recursive (optimal estimation) algorithms are developed for combining multiple attitude measurements obtained from different observation points (i.e., antenna locations), and their efficiencies are tested in various dynamic conditions. The proposed algorithms converge rapidly and produce the required output even during high dynamics manoeuvres. Results of theoretical performance analysis and simulation activities are presented in this paper, with emphasis on the advantages of the GNSS interferometric approach in UAV applications (i.e., low cost, high data-rate, low volume/weight, low signal processing requirements, etc.). Modelling and simulation activities focussed on the AEROSONDE UAV platform and considered the possible augmentation provided by interferometric GNSS techniques to a low-cost and low-weight/volume integrated navigation system recently developed at Cranfield University, which employs a Vision-based Navigation (VBN) system, a Micro-Electro-mechanical Sensor (MEMS) based Inertial Measurement Unit (IMU) and code-range GNSS (i.e., GPS and GALILEO) for position and velocity computations. The integrated VBN-IMU-GNSS (VIG) system is augmented by using the inteferometric GNSS Attitude Determination (GAD) and a comparison of the performance achievable with the VIG and VIG/GAD integrated Navigation and Guidance Systems (NGS) is presented. Finally, the data provided by these NGS are used to optimise the design of an hybrid controller employing Fuzzy Logic and Proportional-Integral-Derivative (PID) techniques for the AEROSONDE UAV.

Keywords: *GNSS Attitude Determination, Interferometry, Unmanned Aerial Vehicle, Low-cost Navigation Sensors, Fuzzy Logic Controller, PID Controller.*

1. INTRODUCTION

Technological developments in the realm of satellite navigation have led to innovative concepts in the mission management of current and next generation air, land and sea vehicles. Navigation systems including GNSS or integrated GNSS/INS are being used extensively today in most aerospace platforms around the world and new promising technologies are being explored. The great majority of current manned and unmanned aerial vehicles perform attitude determination tasks by using inertial sensors (ring laser gyros, fibre optics gyros, accelerometers, etc.), packaged into Attitude and Heading Reference Systems (AHRS) or into Inertial Navigation Systems (INS). Although AHRS/INS technologies are well established [1], they have some disadvantages. High accuracy class products are costly when compared with emerging alternative technologies (e.g., MEMS based Inertial Measurement Units), AHRS/INS position data accuracy degrades with time and their attitude accuracy is strongly dependent on platform dynamics. Furthermore, a significant amount of data processing is required to "smooth-out" sensor errors and extensive simulation, laboratory and ground/flight test activities are often required in order to properly design and calibrate the Kalman Filter parameters. The use of inexpensive GNSS technology for aiding AHRS/INS has been extensively investigated over the past decades, and integrated GNSS/INS systems are the state-of-the-art for aerospace platform navigation applications [2, 3, 4].

The concept of replacing traditional attitude sensors with GNSS interferometric processing (carrier-phase) has been also considered in recent years, mostly for spacecraft applications (replacing or aiding traditional sun-sensors, horizon-trackers, star-trackers, magnetometers, etc.), and for manned aircraft [6, 7, 8] and ship applications [9]. Due to the low volume/weight of current carrier-phase GNSS receivers, and the extremely high accuracy attainable notwithstanding their lower cost, interferometric GNSS technology is becoming an excellent candidate for future UAV applications [10]. The accuracy of the GNSS Attitude Determination (GAD) systems is affected by several factors including the selected equipment/algorithms and the specific platform installation geometry, with the baseline length and multipath errors being the key elements dominating GAD systems performance [10,11]. One of the main challenges of implementing GAD systems for attitude determination in UAV and other

aerospace platforms is the need of resolving integer ambiguity in real-time in order to obtain reliable attitude estimations [10]. In recent years several techniques have been developed for integer ambiguity resolution. Giorgi and Teunissen [12] developed an extension of the known Least-squares Ambiguity Decorrelation Adjustment (LAMBDA) method [13] for solving nonlinearly constrained ambiguity resolution problems associated to GNSS attitude determination. In terms of data rate, Pinchin [10] suggests that a typical AHRS/INS system provides attitude measurements upwards of 100Hz whereas a GAD system output is in the order of 1-5Hz which is too low for high dynamics platform applications. In small UAV platforms a simple solution that integrates a low cost GNSS/MEMS-IMU system for attitude determination may be also affected by vibrations and aerodynamic effects acting on the platform itself (e.g., aeroelasticity). Therefore, a very accurate initial heading estimate or integration with other sensors is often required for stable filter performance in such applications [13]. As a consequence, the integration of additional augmenting sensors such as Vision-based Navigation (VBN) sensors [14, 15] can provide significant improvements in the accuracy and continuity of the measurements. Several methods have been developed in the past decades for GAD systems. The classical method, developed by Cohen [16], involves two main steps. The first step is to find a matrix that transforms the baseline configurations to an equivalent orthonormal basis and the second step is the use of fast algorithms (e.g., QUEST and FOAM) for attitude determination. An alternative method is to adopt recursive algorithms to minimize a cost function that links all available carrier phase measurements. Independently from the method selected, since GAD errors are dominated by lengths of the baselines used, some efficient geometric algorithms are proposed for baseline selection in the presence of redundant satellite measurements. Various controller schemes have also been applied in the past to the design of autonomous control/servoing systems for UAVs. Some of these techniques include Adaptive Control [17, 18, 19], Fuzzy Control [17, 20], Neural Networks, Genetic Algorithms and Lyapunov Theory [21]. Beyond studying the possible synergies attainable from integration of GAD systems with other low-cost and low-weight/volume navigation sensors (e.g., VBN and MEMS-INS), and additional objective of our research is to develop an hybrid Fuzzy/PID controller using INS, GNSS and GAD input data and also capable of VBN guidance (visual servoing) during the final approach and landing phases of the flight. This is allowing the development of an integrated Navigation and Guidance System (NGS) capable of providing the required level of performance in all flight phases of a small UAV.

2. GNSS ATTITUDE DETERMINATION

The fundamental concept of interferometric GNSS Attitude Determination (GAD) is shown in Fig. 1. The measurement of the phase of the GNSS signal carrier allows to determine the relative displacement of the antennae in the body reference frame. This information is directly related to the attitude of the vehicle.

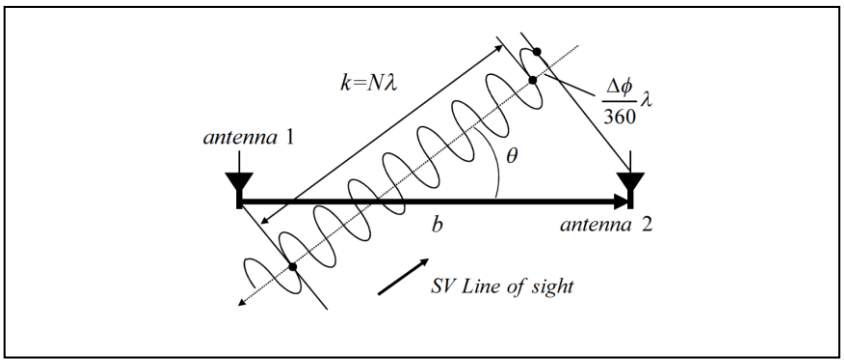

Figure 1: Interferometric GNSS principle.

The displacement of the antenna baseline (b) with respect to the LOS of the GNSS signal is given by:

$$\theta = \cos^{-1}\left[\frac{k + \frac{\Delta\phi}{360}}{b} \cdot \lambda\right] \quad (1)$$

where the phase difference $\Delta\phi/360$ is proportional to the projection of the baseline (b) on the Line-of-Sight (LOS). Since the antennae are placed at different locations, the phase measurements of the incoming GNSS signal carrier are different for each antenna. By knowing the integer number of cycles travelled by the

carrier (N), it is possible to determine the vehicle attitude. The use of GNSS for position determination requires that the vehicle is able to "see" at least 4 satellites in order to solve a system of four equations with four unknowns (i.e., platform coordinates and delta-time). When using GNSS for attitude determination it is sufficient that only two satellites are in view due to the following considerations:

- Common time reference: measurements are independent from the error at the receiver clock as it is the same for the measurements performed by each antenna.
- Baseline setting: the relative position of the antennae on the vehicle is known a priori; this eliminates another unknown factor which reduces the number of satellites required.

2.1 GAD Algorithms

Knowing the coordinates, both in the body reference frame and in the North-East-Down (NED) frame, of the unit vectors of the LOS to the S_n satellites, and the unit vector perpendicular to the plane containing three antennae $\hat{A}$, it is possible to determine the attitude of the vehicle. In the body axis reference frame (x, y, z) any combination of 3 not aligned antennae located at the points P_1, P_2, P_3 originates a plane $\boldsymbol{\pi}$. This plane is the locus of points P with coordinates that satisfy the equation:

$$\begin{vmatrix} x & y & z & 1 \\ x_1 & y_1 & z_1 & 1 \\ x_2 & y_2 & z_2 & 1 \\ x_3 & y_3 & z_3 & 1 \end{vmatrix} = 0 \qquad \begin{vmatrix} x-x_1 & y-y_1 & z-z_1 \\ x_2-x_1 & y_2-y_1 & z_2-z_1 \\ x_3-x_1 & y_3-y_1 & z_3-z_1 \end{vmatrix} = 0 \rightarrow \; ax+by+cz+d=0 \tag{2}$$

Since the plane $\boldsymbol{\pi}$ is represented by equation $ax + by + cz + d = 0$, the vector of components (a, b, c) is orthogonal to the plane. Therefore, the coordinates of the unit vector $\hat{A}$ orthogonal to the plane are:

$$A_x = \frac{a}{\sqrt{a^2+b^2+c^2}}; \quad A_y = \frac{b}{\sqrt{a^2+b^2+c^2}}; \quad A_z = \frac{c}{\sqrt{a^2+b^2+c^2}} \tag{3}$$

From the three antennae located on the plane $\boldsymbol{\pi}$, a master antenna M and two "slaves" B with components (B_1, B_2, B_3) and C with components (C_1, C_2, C_3) are defined (Fig. 2).

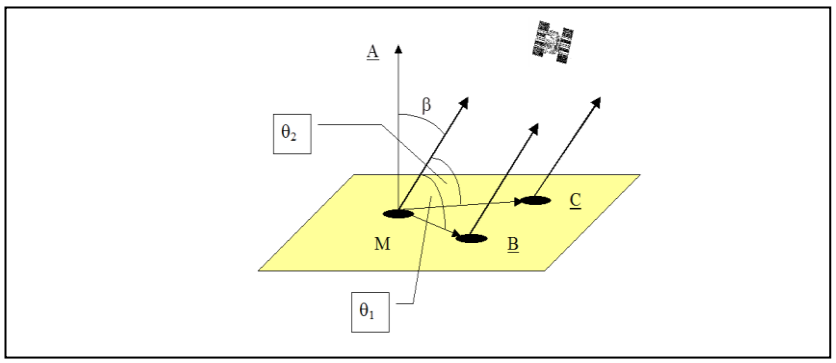

Figure 2: Master and slave antennae.

Using the relations to determine the angle between two vectors and between a vector and a plane, the unit vectors from the LOS to satellites (S_n) are those for which the following conditions apply:

$$\cos\theta_1 = \frac{B_1S_1 + B_2S_2 + B_3S_3}{\sqrt{B_1{}^2 + B_2{}^2 + B_3{}^2}\sqrt{S_1{}^2 + S_2{}^2 + S_3{}^2}} \tag{4}$$

$$cos\,\beta = sin\,S\pi = \frac{aS_1 + bS_2 + cS_3}{\sqrt{a^2+b^2+c^2}\sqrt{S_1{}^2 + S_2{}^2 + S_3{}^2}} \tag{5}$$

$$\cos\theta_2 = \frac{C_1S_1 + C_2S_2 + C_3S_3}{\sqrt{C_1{}^2 + C_2{}^2 + C_3{}^2}\sqrt{S_1{}^2 + S_2{}^2 + S_3{}^2}} \tag{6}$$

$$\cos\beta = \frac{A_1S_1 + A_2S_2 + A_3S_3}{\sqrt{{A_1}^2 + {A_2}^2 + {A_3}^2}\sqrt{{S_1}^2 + {S_2}^2 + {S_3}^2}} \tag{7}$$

From Eq. (5) and Eq. (7), a system of 3 equations with 3 unknowns (S_1, S_2, S_3) is obtained only if the magnitude of the LOS vector is known . The unknowns are the coordinates of vector LOS in the body frame. Then, the angle β, which is the angle between the LOS vector to the satellite $\hat{S}_n$ and the perpendicular $\hat{A}$ to the plane $\boldsymbol{\pi}$, can be obtained directly from equations Eq. (5) and Eq. (7). The unit vectors $\hat{S}_n \rightarrow$ LOS, known in the body frame, are fully defined in the NED frame (CG, x_N, y_N, z_N). In fact, the receiver extracts the coordinates of the satellite from the navigation message. From these parameters, it computes the unit vector of the LOS in ECI frame. Since the NED frame is always defined with respect to the ECI-frame the unit vectors $\hat{S}_N$ are then properly defined in the NED frame. In particular if C_E^N is the transformation matrix from ECI-frame to NED, the unit vector $\hat{S}_{n_N}$ in the NED frame is given by the following transformation:

$$\hat{S}_{n_N} = \begin{bmatrix} S_{x_N} \\ S_{y_N} \\ S_{Z_N} \end{bmatrix} = C_E^N \begin{bmatrix} S_{X\,ECI} \\ S_{Y\,ECI} \\ S_{Z\,ECI} \end{bmatrix} \tag{8}$$

The next step is to determine the coordinates of $\hat{A}$ in the NED frame in order to have a full set of vectors that will be used for attitude determination. The geometry illustrated in Fig. 3 is obtained.

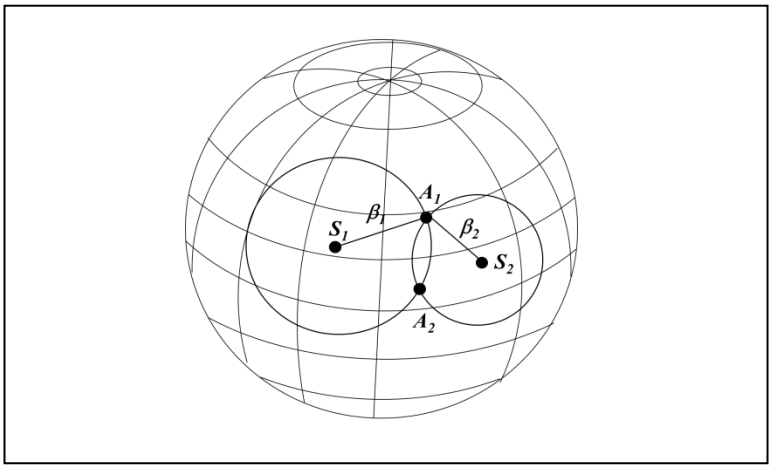

Figure 3: Geometry with two satellites.

Analytically this geometric problem can be represented by a system of 3 equations with 3 unknowns A_1, A_2, A_3. These are the components of vector A in the auxiliary reference frame (x_1, x_2, x_3):

$$\begin{cases} \hat{\mathrm{A}} \cdot \hat{\mathrm{S}}_1 = \cos\beta_1 \\ \hat{\mathrm{A}} \cdot \hat{\mathrm{S}}_2 = \cos\beta_2 \\ \hat{\mathrm{A}} \cdot \hat{\mathrm{A}} = 1 \end{cases} \tag{9}$$

By getting:

$$p = \frac{\cos\beta_1 - \hat{S}_2 \cdot \hat{S}_1 \cos\beta_2}{1 - \left(\hat{S}_2 \cdot \hat{S}_1\right)^2}; \quad q = \frac{\cos\beta_2 - \hat{S}_2 \cdot \hat{S}_1 \cos\beta_1}{1 - \left(\hat{S}_2 \cdot \hat{S}_1\right)^2}; \quad r = \pm\sqrt{\frac{1 - p\cos\beta_1 - q\cos\beta_2}{1 - \left(\hat{S}_2 \cdot \hat{S}_1\right)^2}} \tag{10}$$

the solution of $\hat{A}$ becomes:

$$\hat{A} = p\,\hat{S}_1 + q\,\hat{S}_2 + r\,\hat{S}_x \tag{11}$$

Eq. (11) generates 2 possible ambiguous solutions. In order to solve this ambiguity the following steps can be performed:

- Compare the possible solution with an estimation made in advance.
- Compare more attitude solutions that can be accumulated in a certain observation time discarding those which are dispersed.
- Use a third satellite.

Fig. 4 shows the geometry obtained by including a third satellite in the solution.

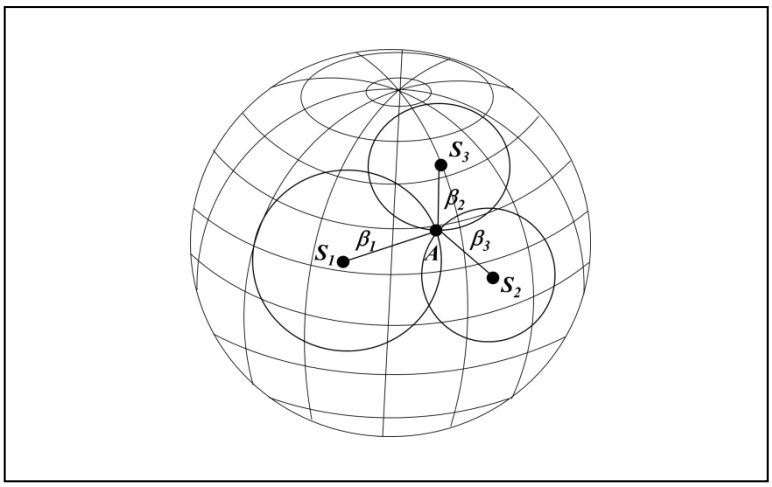

Figure 4: Addition of a third satellite to the solution of $\hat{A}$.

The analytical solution of the system illustrated in Fig. 4 is given by:

$$\begin{cases} \hat{A}\cdot\hat{S}_1 = \cos\beta_1 \\ \hat{A}\cdot\hat{S}_2 = \cos\beta_2 \\ \hat{A}\cdot\hat{S}_3 = \cos\beta_3 \\ \hat{A}\cdot\hat{A} = 1 \end{cases} \rightarrow \begin{cases} \hat{A} = p\,\hat{S}_1 + q\,\hat{S}_2 + r\,\hat{S}_x \\ \hat{A}\cdot\hat{S}_3 = \cos\beta_3 \end{cases} \tag{12}$$

Although the system Eq. (12) has a unique solution for $\hat{A}$ in a real system it is necessary to take into account the possible errors in the determination of the values of $\hat{S}_n$ and β_n as illustrated in Fig. 5.

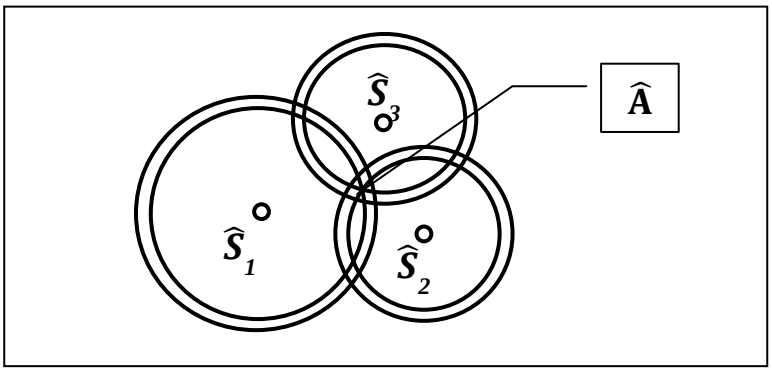

Figure 5: Errors in the determination of $\hat{S}_n$ for the computation of $\hat{A}$.

With the methodology described above, the input data required to determine the attitude states of the vehicle is defined (i.e., the coordinates of the vectors $\hat{S}_n$ and the coordinates of the vectors $\hat{A}$ in the body frame and in the NED frame). Then two approaches can be used for attitude determination, one is a variant of the classical method [16] that allows the determination of the attitude states by considering one single pair of vectors (e.g., $\hat{A}$

and $\hat{S}_1$, $\hat{S}_1$ and $\hat{S}_2$). In order to select the optimal pair of vectors, the errors associated to such combination are considered (the pair with the minimum RMS/RSS error is selected). The second method adopts a recursive algorithm that minimizes a cost function that links all available measurements (e.g., $\hat{A}, \hat{S}_1, \hat{S}_2, \hat{S}_3$). The firs method first determines the vectors $\hat{A}, \hat{S}_1, \hat{S}_2, \hat{S}_3$. Then, assuming that there are at least 3 nonaligned antennae and 2 or 3 GNSS satellites in view, a pair of vectors from $\{\hat{S}_1, \hat{S}_2, \hat{S}_3\}$, associated with the minimum error is selected. The total error is calculated for vector $\hat{A}$, In this way the associations of two pairs of vectors: ($\hat{A}_B$, $\hat{S}_{1B}$) and ($\hat{A}_I$, $\hat{S}_{1I}$) or (S_{1B}, $\hat{S}_{2B}$) and ($\hat{S}_{1I}$, $\hat{S}_{2I}$) are formed. Such associations are named as follows:

$$\begin{gathered}(\hat{A}_B\ ,\ \hat{S}_{1B}\ )\ ;\ (\ \hat{S}_{1B}\ ,\ \hat{S}_{2B}\ )\ =\ \widehat{W}_1\ ,\widehat{W}_2 \text{ - Body axes reference frame} \\ (\hat{A}_b\ ,\ \hat{S}_{1I}\ )\ ;\ (\ \hat{S}_{1I}\ ,\ \hat{S}_{2I}\ )\ =\ \hat{V}_1\ ,\hat{V}_2 \text{ - Inertial reference frame}\end{gathered} \tag{13}$$

Assuming the absence of measurement errors, the following equations can be written:

$$\widehat{W}_1 = C\hat{V}_1; \quad \widehat{W}_2 = C\hat{V}_2 \tag{14}$$

where C is the direct cosine matrix (i.e., from attitude angles). In theory, these two equations can be combined:

$$\widehat{W}_1 \cdot \widehat{W}_2 = \hat{V}_1 \cdot \hat{V}_2 \tag{15}$$

However, due to measurement errors this equality cannot be verified in general. Nevertheless, it is possible estimate the vehicle attitude by employing the simple algorithm described below. This deterministic algorithm uses a subset of the available data. Following the discussion, two orthonormal triads of vectors can be obtained:

$$\hat{r}_1 = \hat{V}_1, \qquad \hat{r}_2 = \frac{\hat{V}_1 \times \hat{V}_2}{\left|\hat{V}_1 \times \hat{V}_2\right|}, \qquad \hat{r}_3 = \hat{r}_1 \times \hat{r}_2 \tag{16}$$

$$\hat{s}_1 = \widehat{W}_1, \qquad \hat{s}_2 = \frac{\widehat{W}_1 \times \widehat{W}_2}{\left|\widehat{W}_1 \times W_2\right|}, \qquad \hat{s}_3 = \hat{s}_1 \times \hat{s}_2 \tag{17}$$

From Eq. (14), Eq. (15) and Eq. (16):

$$\hat{s}_i = C\hat{r}_i \qquad i = 1,2,3 \tag{18}$$

It is not possible to find a proper orthonormal matrix (i.e., det $|C|$ = 1) that satisfies Eq. (14). Nonetheless, is always possible to determine a matrix that satisfies equation Eq. (18) from which results:

$$\begin{gathered}\hat{s}_i \cdot \hat{s}_j = \hat{r}_i \cdot \hat{r}_j = \delta_{ij} \quad i,j = 1,2,3 \\ \delta_{ij} = \begin{cases}1, & if\ i = j \\ 0 & if\ i \neq j\end{cases}\end{gathered} \tag{19}$$

The orthonormal column matrices are:

$$A \equiv [\hat{s}_1 \quad \hat{s}_2 \quad \hat{s}_3], \quad B \equiv [\hat{r}_1 \quad \hat{r}_2 \quad \hat{r}_3] \tag{20}$$

and:

$$A = CB \tag{21}$$

Since B is a proper orthonormal matrix, multiplying both sides of the equation by B^T results in:

$$C = AB^T \tag{22}$$

Since A is not satisfied in general, Eq. (22) cannot provide an exact solution of the vehicle attitude (i.e., attitude calculated from real data is always subject to errors). However, if we consider the error in the data, the described method always allows to determine a proper orthogonal matrix C. By constructing C the components of $\hat{W}_2$ and $\hat{V}_2$ that might violate the equality expressed in Eq. (15) are eliminated. Although the traditional method allows to obtain a single solution, it is not the unique possible solution. In fact, by inverting the order of the observation vectors ($\hat{S}$ to the place of $\hat{A}$ and vice versa) the algorithm leads to a different (but very similar) solution. Then, the uniqueness of the solution is achieved by specifying the order of the two vectors. Since the inaccuracy of the data for the second vector ($\hat{W}_2$ and $\hat{V}_2$) is absorbed by the algorithm, a more accurate attitude estimation is obtained by choosing a more accurate first vector ($\hat{W}_1$ and $\hat{V}_1$). Therefore, if $\hat{S}_1$ and $\hat{S}_2$ are the selected observation vectors, it is appropriate to select as first the one measured using the longest baseline. In the case of using vectors $\hat{A}$ and $\hat{S}_n$ it is also appropriate to choose the vector $\hat{S}_n$ as the first, because with three satellites in view, vector $\hat{A}$ is, in general, less accurate as it is calculated by using the three vectors $\{\hat{S}_1, \hat{S}_2, \hat{S}_3\}$ and the error is, to a first approximation, additive. Theoretically, however, there may be cases in which the error of $\hat{A}$ is less than the error of $\hat{S}_n$. The second method (recursive algorithm), uses all available information from 3 nonaligned antennae and 3 satellites ($\hat{A}, \hat{S}_1, \hat{S}_2, \hat{S}_3$), to obtain an estimation of the attitude of the vehicle by minimizing the following cost function:

$$CJ[C] = \frac{1}{2}a_1\left|A_b - C\hat{A}_i\right|^2 + \frac{1}{2}a_2\left|\hat{S}_{1b} - C\hat{S}_{1i}\right|^2 - \frac{1}{2}a_3\left|\hat{S}_{2b} - C\hat{S}_{2i}\right|^2 + \frac{1}{2}a_4\left|\hat{S}_{3b} - C\hat{S}_{3i}\right|^2 \quad (23)$$

where a_1, a_2 and a_3 and a_4 are 4 non-negative weights. Therefore, for a number of N measurements, such a cost function can be generalized as follows:

$$J[C] = \frac{1}{2}\sum_{k=1}^{N} a_k\left|\hat{W}_k - C\hat{V}_k\right|^2 \quad (24)$$

where $\hat{W}_k$is a vector determined in the body axis frame and $\hat{V}_k$is the corresponding vector in the inertial frame. In the ideal case of absence of errors, each term of Eq. (23) would be cancelled in correspondence to a certain proper orthogonal matrix C. As this does not occur in reality, it is necessary to assign appropriate weights in order to minimize the cost function by considering the accuracy of the measurements. Since only 3 of 9 elements are independent, it is acceptable to minimize the cost function for a minimum number of parameters (e.g., Euler angles), in order to reduce the complexity on the calculation.

2.2 GAD Accuracy

Similarly to Geometric Dilution of Precision (GDOP, the Attitude Dilution of Precision (ADOP) is a parameter that indicates how accurate the attitude solution is. The ADOP is related to the error in attitude calculation σ_θ, the error in range σ_r and the baseline length b by the following equation:

$$\sigma_\theta = \text{ADOP} \cdot \frac{\sigma_r}{b} \quad (25)$$

where:

$$\text{ADOP} = \sqrt{\text{trace}[(nI - SS^T)^{-1}]} \quad (26)$$

and $S = [s_1, s_2, \ldots s_n]$ is the matrix $(1 \times n)$ of the LOS to the satellite, n is the number of satellites in view and I the identity matrix. The value of ADOP is generally equal to 1 or less. This indicates that the GNSS constellation guarantees favourable geometry for the attitude determination. Therefore, it is possible to make an approximation of the attitude error by assuming that ADOP=1. With this assumption the relationship is simplified to:

$$\sigma_\theta = \frac{\sigma_r}{b} \quad (27)$$

By knowing the error σ_θ associated with each measure, assuming that the measures are statistically independent, it is possible to calculate the total RSS error σ_{TOT} by the relation:

$$\sigma_{TOT} = \sqrt{{\sigma_{\theta 1}}^2 + {\sigma_{\theta 2}}^2 + {\sigma_{\theta 3}}^2} \tag{28}$$

The error in attitude determination is a function of the instantaneous orientation of the aircraft, the satellite geometry and the selected baselines. In Eq. 25 and Eq. 27 the range error σ_r is presented; in order to quantify its value, Table 1. shows typical values for its main components.

Table 1: Components of error in range.

Sources	Error: σ_r
Multipath	~ 5 mm
Structural Distortion	Application Specific
Troposphere	Can be Modelled
Signal to Noise (SNR)	< 1 mm
Error in the Receiver	< 1 mm

Multipath. This is the main source of error. Even though the error is highly deterministic, previous research [22] shows that even with the most careful study on the location of the antennae the error cannot be reduced below the 5 mm threshold. This error is directly dependant on different non-controlled variables such as the environment itself; other variables also influence this source of error, such as materials, antennae gain, geometry, etc. The control of these variables to reduce the error is often complex and expensive.

Structural distortion. In high temperature applications the vehicle surface may experience thermal deformation. This will cause a relative displacement between antennae with consequent errors in the attitude solution. Aeroelastic effects also introduce structural distortions.

Tropospheric error. The troposphere is often considered a source of error for the transmission of electromagnetic signals [23, 24]. As illustrated in Fig. 6, the error becomes more significant with the increase of the refraction index. This increase becomes significant at altitudes $h < 10\text{Km}$. The refraction index causes a deflection of the GNSS signal [25]. The refraction index can be modelled according to Snell's law:

$$\frac{\sin\theta_1}{\sin\theta_2} = \frac{n_1}{n_2} \tag{29}$$

where $n_1 = 1$, $n_2 \approx 1.00026$ and $n_2 = f(\rho, V)$. It can be observed that tropospheric error causes the GNSS signal to appear coming from a different direction from the satellite. Therefore an error is introduced when the phase measurements are converted to attitude angles.

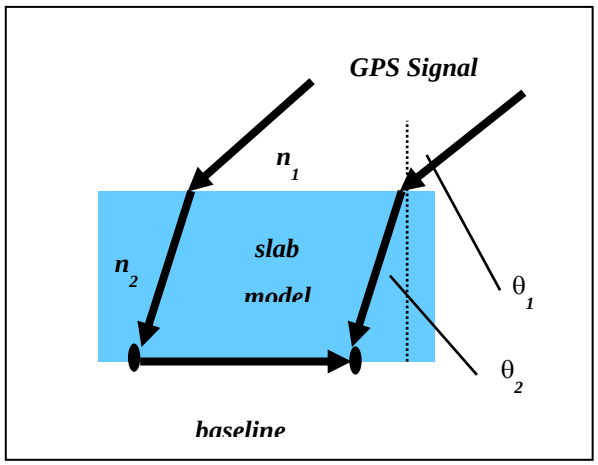

Figure. 6: Tropospheric error.

Signal-to-Noise Ratio (SNR). In high dynamics applications the tracking loop bandwidth needs to be extended. By extending it, the bandwidth of the associated error is also increased [26]. Many stochastic models have been proposed based on the SNR reported by the receiver [27, 28]. In this case, the SNR is modelled as

$$\sigma_{SNR} = \sqrt{\frac{f_N}{C/N_0}}\ \frac{\lambda}{2\pi} \tag{30}$$

where f_N is the noise of the carrier tracking loop and the ratio C/N_0 is the carrier-noise ratio. Typically, these parameters have the following values: $f_N = 10$Hz, $c/N_0 = 40$dB-Hz, so that $\sigma_{SNR} < 1$m.

Specific errors in the receiver. This source of error can become significant if it is not considered at an early design stage. Nowadays, technology allows to have precise models of it [22, 29]. There are several examples of those errors such as crosstalk, which is common in antennae with high gain, line bias, which is the phase offset between one antenna and another and inter-channel bias, which results of the phase measurements from different satellites that use a different channel.

Total error. From the analysis on the different source of errors in range, considering that multipath is the dominant error, a rough approximation to this error is given by :

$$\sigma_\theta(\text{rad}) \cong 0.5/\text{L (cm)} \tag{31}$$

where L is the longitude of a given baseline. In Eq. (31), it is shown that the error appears inversely proportional to the length of the baseline used for attitude determination. Hence it is always preferred to use longer baselines which allow a more accurate attitude solution. A detailed discussion of the sources of errors can be found in the literature [30, 31].

2.3 Geometric Algorithm for Antennae Selection

As a first step the antennae with less than 2 satellites in view are discarded by using a masking algorithm. It is then when the baselines are measured between the remaining antennae.

$$\vec{b} = \vec{a}_0 - \vec{a}_1 \tag{32}$$

By ordering the baselines in descending order there is a selection of the first two that are associated with the greater area of the triangle formed by the baselines and their links. The common antenna with respect to these baselines is identified as possible Master M antenna while the other two are possible slaves: Sl_1 and Sl_2. Once the process is repeated for all antennae with at least 2 satellites in view the optimal combination of three antennae is selected for those, whose the following function is maximum:

$$R = \frac{\rho_1 + \rho_2}{\rho_1 - \rho_2} \tag{33}$$

Where $\rho_1$and $\rho_2$are the lengths of baselines $M - Sl_1$ and $M - Sl_2$. This algorithm is illustrated in Fig. 7.

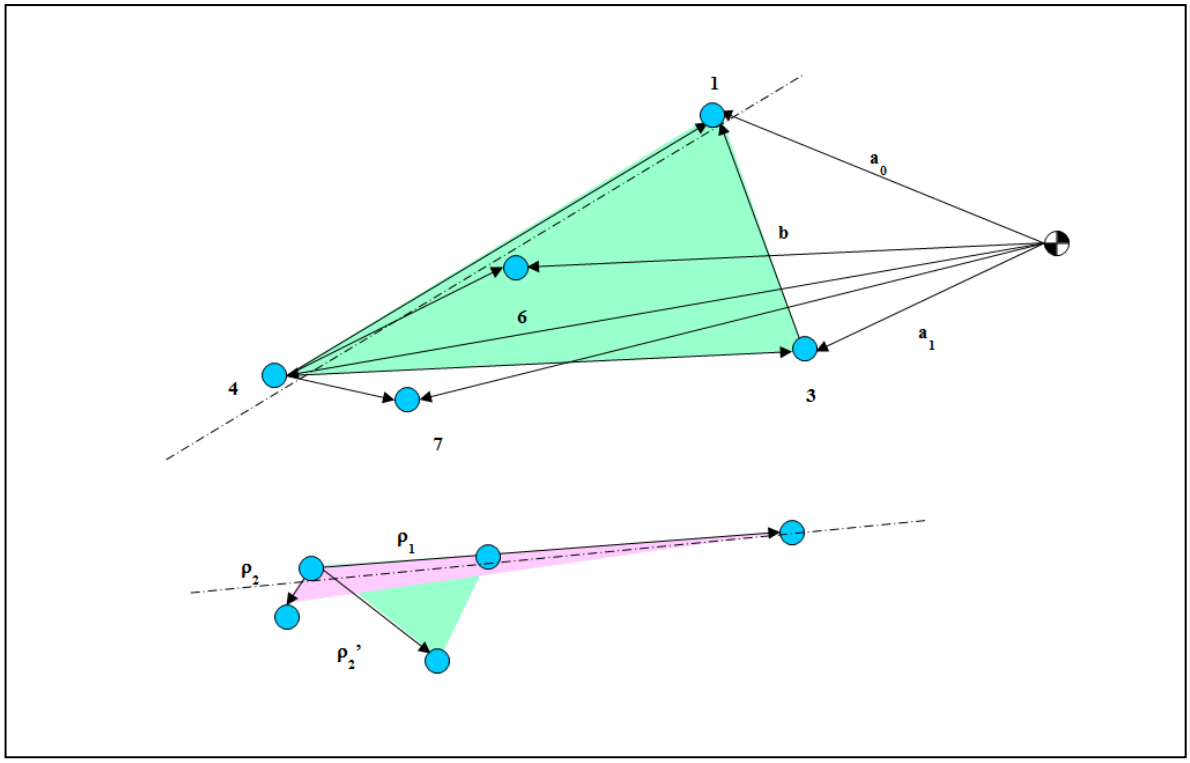

Figure7: Geometric Algorithm for a Combination of 3 antennae with at least 2 satellites in view.

3. MULTISENSOR DATA FUSION

The next step is to integrate the GNSS/GPS attitude determination system to the VIG Navigation System illustrated in Fig. 8. This navigation system includes a VBN navigation system, an inertial navigation system and a GNSS system for position determination. The details of the development of this NGS can be found in [14, 15].

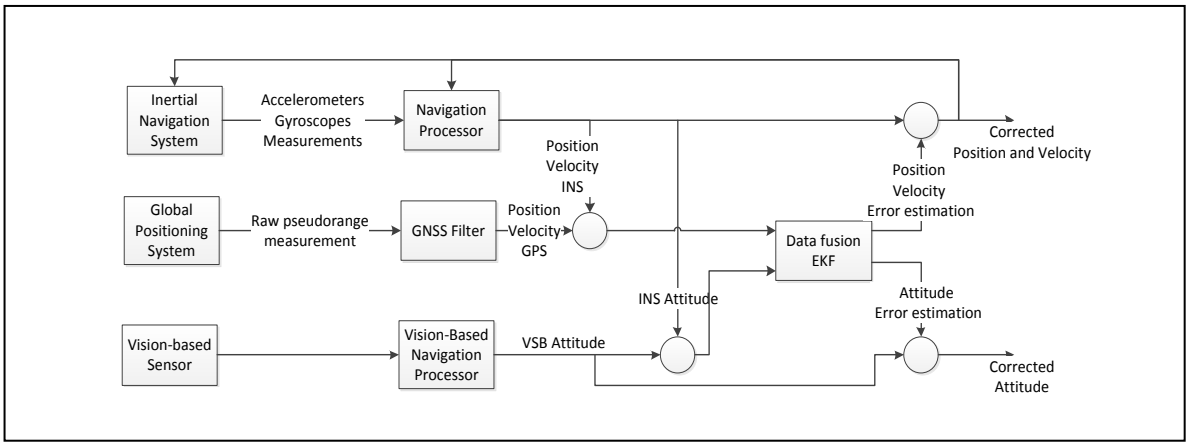

Figure 7: INS/GPS/VBS Integration.

Employing the geometric algorithm for optimal selection of the antenna baselines and the recursive algorithm (Eq. 23 - 24) for over-determined attitude computations, the resulting error analysis is presented in Table 6.

Table 6: GNSS attitude determination errors.

Configuration	1-σ Pitch Error (°)	1-σ Roll Error (°)	1-σ Yaw Error (°)
3 Antennae	1.37	0.93	1.77
4 Antennae	0.47	0.32	0.76
5 Antennae	0.38	0.52	0.54
6 Antennae	0.32	0.45	0.36
7 Antennae	0.29	0.34	0.31
8 Antennae	0.27	0.23	0.22

Then the GNSS attitude determination is integrated to the VIG Navigation System as Illustrated in Fig. 9.

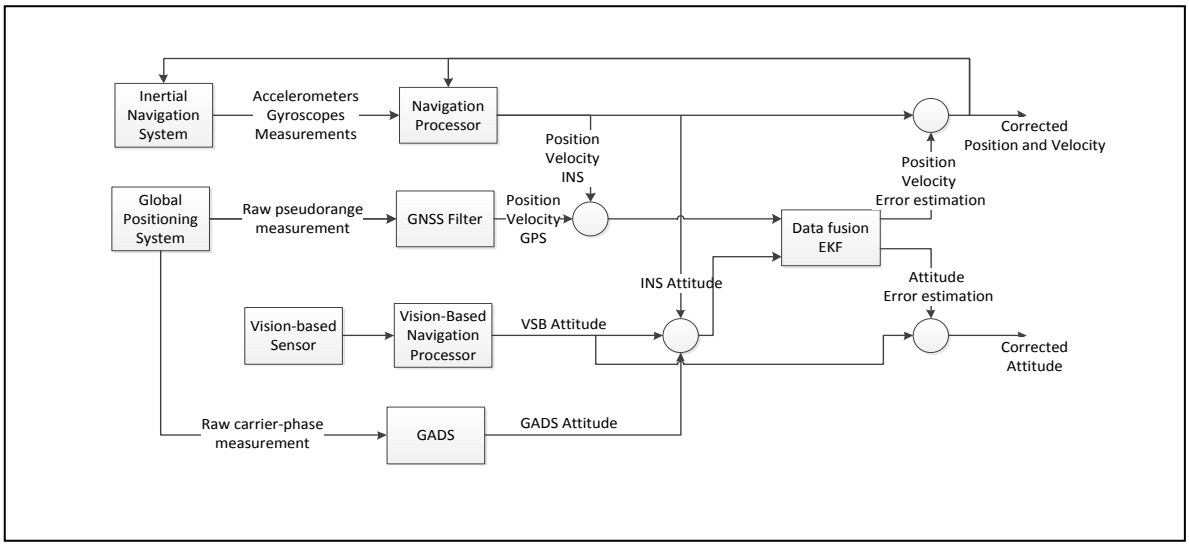

Figure 9: GNSS Attitude Algorithm Integrated to VIG Navigation System.

It can be observed that the output of the GNSS Attitude Determination System (GAD) is integrated to the navigation system extended Kalman Filter for data fusion. The details of the EKF implementation can be consulted in [14, 15].

4. CONTROLLER DESIGN

The AEROSONDE model from Unmanned Dynamics LLC was used in the simulation. The AEROSONDE UAV is a small autonomous aircraft used in weather-reconnaissance and remote-sensing missions. Its main characteristics are listed in Fig. 10.

- **Wingspan: 2.9 m**
- **Weight: 13 -15 kg (29-33 lbs.)**
- **Engine: 24cc fuel injected, premium unleaded gasoline**
- **Battery: 20 W-hr**
- **Fuel tank: 5 kg when full**
- **Speed: 80-150 km/hr (50-93 miles/hour) cruise, 9 km/hour (6 miles/hr) climb**
- **Range: > 3,000 km distance, > 30 hours, 0.1-6 km altitude (depending on payload)**
- **Payload: up to 2 kg (4.4 lbs.) with full fuel load**
- **Navigation: GPS**
- **Communications: UHF radio or LEO satellite**
- **Material: carbon fiber**
- **Propeller: Real propeller**

Figure. 10 AEROSONDE UAV Characteristics [33].

This model is part of the AeroSim Blockset implemented in Matlab/Simulink. The AeroSim Blockset provides components for rapid development of non-linear 6-DOF dynamic models [32]. In addition to the basic dynamic blocks, complete aircraft models are present which can be configured as required. The library also includes Earth models (geoid references, gravity and magnetic fields) and atmospheric models. The AEROSONDE UAV model can be interfaced with simulators such as Flight-Gear and MS Flight Simulator to allow visualisation of the aircraft trajectory. The inputs to the AEROSONDE model include control surface deflections in radians, throttle input, mixture and ignition. Wind disturbances can be added to the model to simulate variable atmospheric conditions. The model outputs the various aircraft states such as the position in the Earth-fixed frame, attitude and attitude rates. In order to perform the GNSS attitude determination for the AEROSONDE, 5 GNSS antennae were selected in order to optimize the length of the baselines. The baseline lengths are defined in Table 3.

Table 3: Approximate Baseline Length (cm) of Antennae in AEROSONDE UAV.

Antennae	1	2	3	4	5
1		100	180	120	200
2	100		100	100	140
3	180	100		100	100
4	120	100	100		130
5	200	140	100	130	

The position of the antennae in the AEROSONDE can be observed in Fig. 11.

ARPN Journal of Systems and Software

http://www.scientific-journals.org

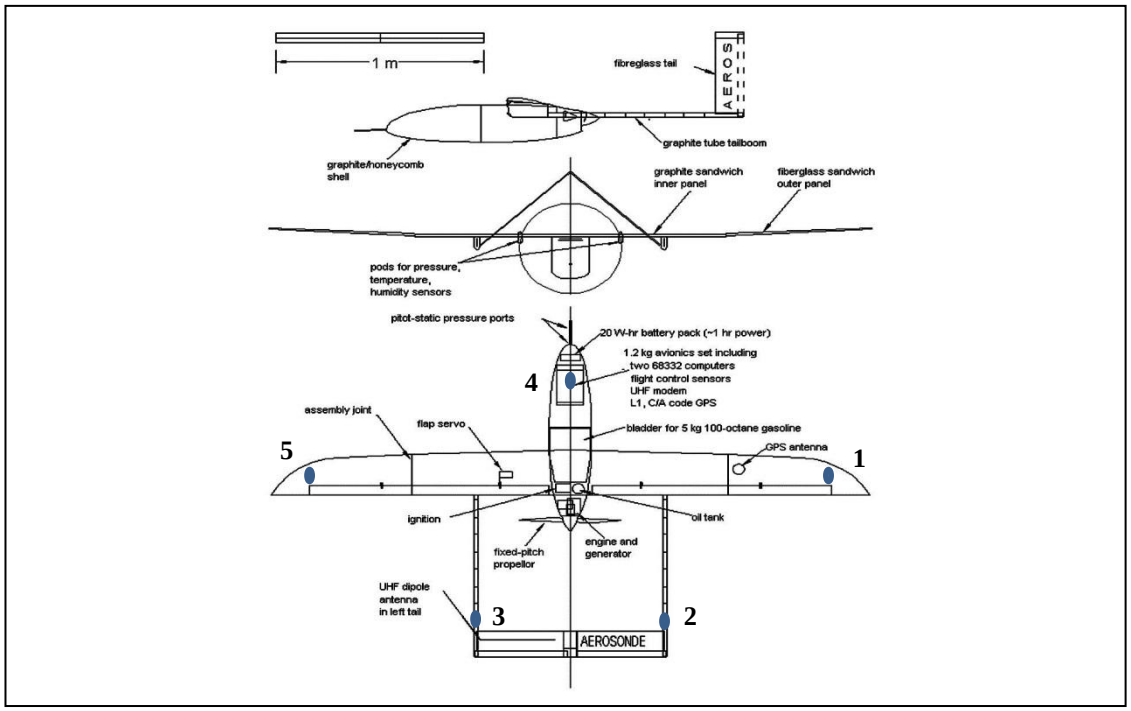

Figure 11: Proposed antennae location adapted from [33].

For the design of the control system, an hybrid approach was adopted allowing the controller to take advantage of the VIG/VIG/GAD integrated navigation sensors during the other phases of flight. To achieve this, fuzzy logic and PID control strategies were adopted for controlling the UAV. PID is the simplest type of linear controller and is used in most UAV control systems. It is easy to implement and is effective for simple systems. The PID control law consists of three basic feedback signals, namely proportional, integral and derivative with gains K_p, K_i and K_d respectively. The values of these gains are often found by trial and error. The required performance and stability can be achieved by adjusting these values. The gains affect the system as follows:

- P term: Increasing K_p speeds up the response of the system. However, high values of the proportional gain can affect the stability of the system. The steady state error is reduced but not eliminated.
- I term: The integral controller eliminates steady state error. It also tends to destabilise the system.
- D term: The derivative controller increases the stability of the system and has no effect on the steady state error. The overshoot of the system is reduced by increasing K_d. Sensor noise is amplified due to this controller.

Fig. 12 shows the PID controller incorporated in a closed loop system with unity negative feedback.

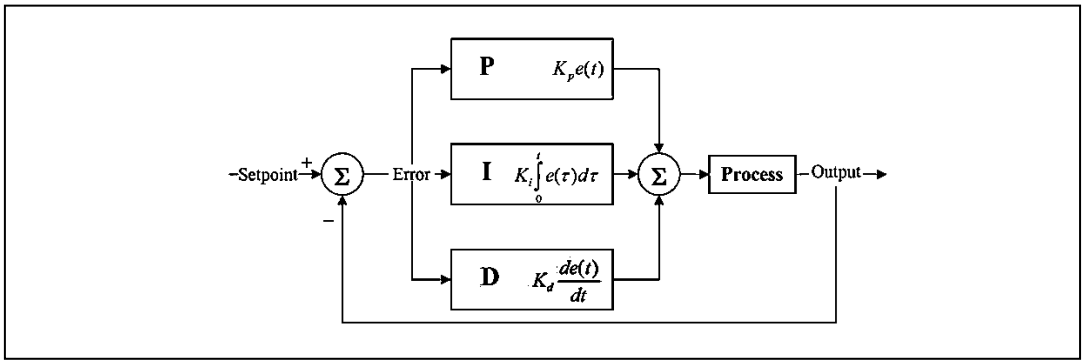

Figure 12: PID controller.

Fuzzy logic is a form of multi-value logic based on a representation of knowledge and reasoning of a human operator. In contrast to conventional PID controllers, Fuzzy Logic Controllers (FLC) do not require a model of the system. Therefore, it can be applied to non-linear systems or various ill-defined processes for which it is

difficult to model the dynamics. The fuzzy logic process is illustrated in Fig. 13.

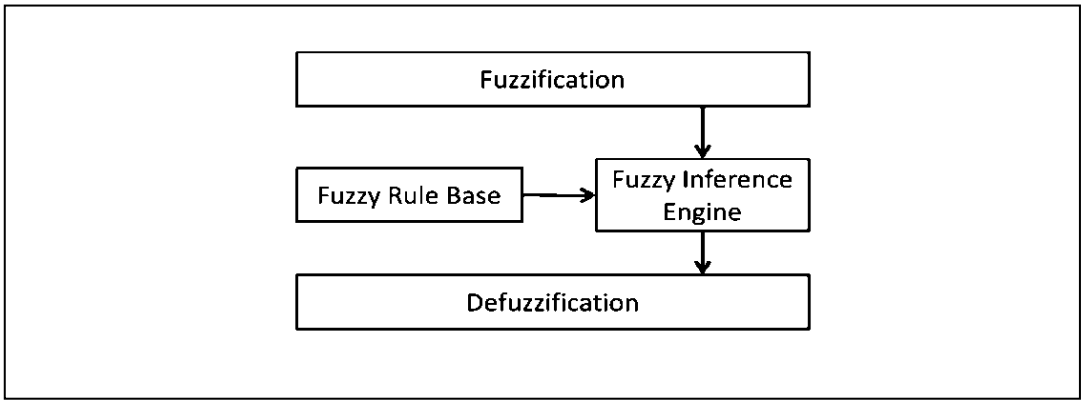

Figure 13: Fuzzy logic system.

The process consists of four components: fuzzification, fuzzy rule base, inference engine and defuzzification. Fuzzification refers to transforming a crisp set into a fuzzy set using linguistic terms. A fuzzy set is a set without crisp, clearly defined boundary. It can contain elements with only a partial degree of membership. A membership function (MF) is defined as a curve that classifies how each point in the input space is mapped to a membership value (or a degree of membership) between 0 and 1. Different types of fuzzy logic membership function exist which include s-function, π-function, z-function, triangular function, trapezoidal function, flat π function rectangle and singleton. An example of this is given in Fig. 14. Let 'input1' be a crisp set for the input to the system with fuzzy sets 'short ', 'medium' and 'long'. Triangular membership functions are used in this case. It is observed that for 'medium', the value 5 has a membership function of 1. The value 3 has a membership function 0.3. Therefore it can be inferred that 3 has a lesser belonging to the fuzzy set 'medium' than 5. Similarly an output function 'output1' is defined with fuzzy sets 'left', 'centre' and 'right' as shown in Fig. 15.

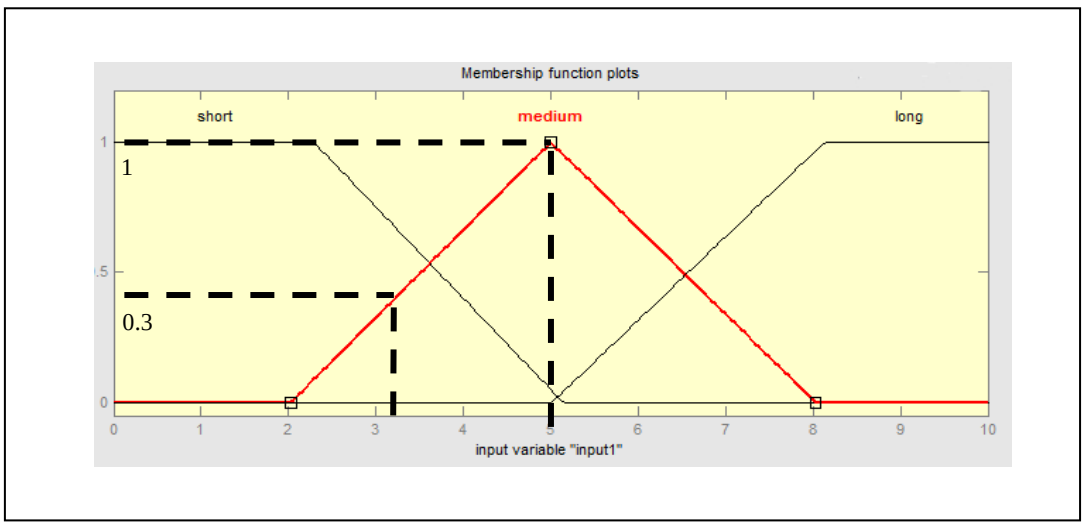

Figure 14: Input fuzzy sets and their membership functions.

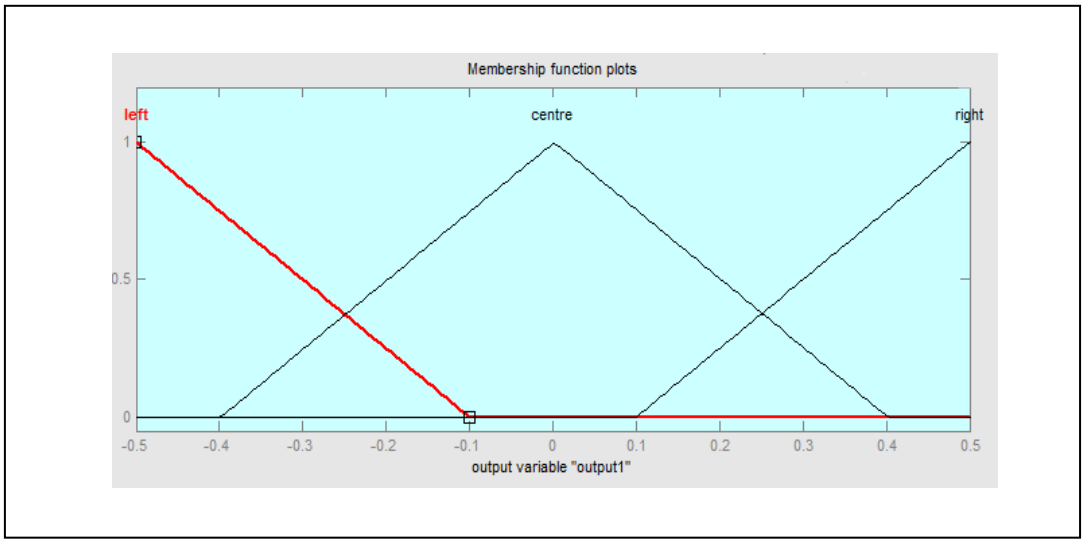

Figure 15: Output fuzzy set and membership functions.

The second component, that is the Fuzzy Rule base, forms the main part of fuzzy logic. It is based on if-then rules that tell the controller how to react to the inputs. The inference engine applies the fuzzy rule base to the inputs and output. It calculates the output required from the rules and passes this to defuzzification. Defuzzification is the method to obtain the output from the controller. It converts the output fuzzy set value to a crisp set using its membership functions.

The UAV controller design was approached by decoupled the dynamic models of the aircraft. This resulted in two complimentary controllers, one for lateral motion and one for longitudinal motion. The functional architecture of the controller is given in Fig. 16.

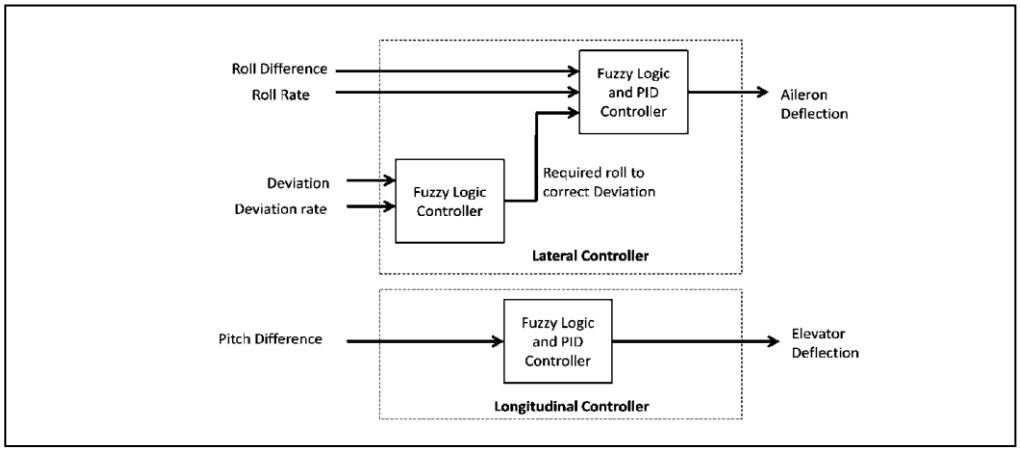

Figure 16: Functional architecture of the controller.

Before initiating the controller design, the open-loop response of the system was first tested. In open-loop flight, the control inputs were set to a fixed value without any feedback from the aircraft states. It is observed that the UAV is unstable in this condition and settles in a constant bank turn and pitch angle as shown in Fig. 17 and Fig. 18. This is due to the propulsion system which causes an unbalanced roll moment and excites the spiral mode.

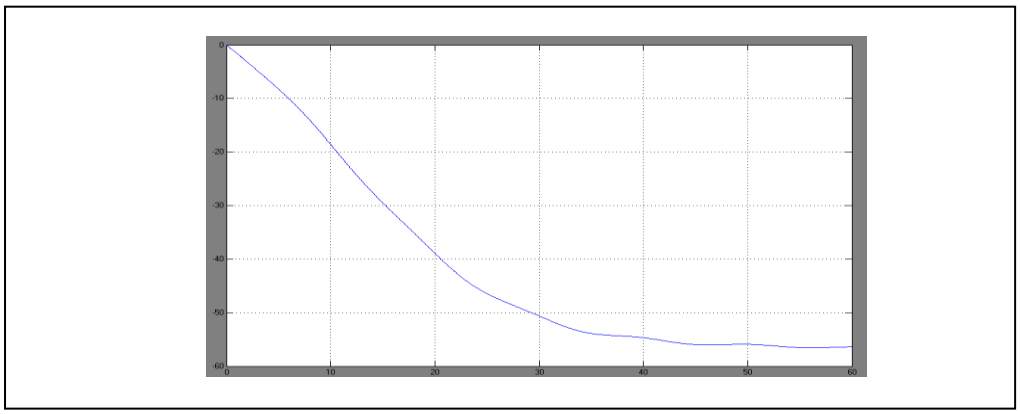

Fig. 17: ϕ (roll) angle open-loop response (spiral mode).

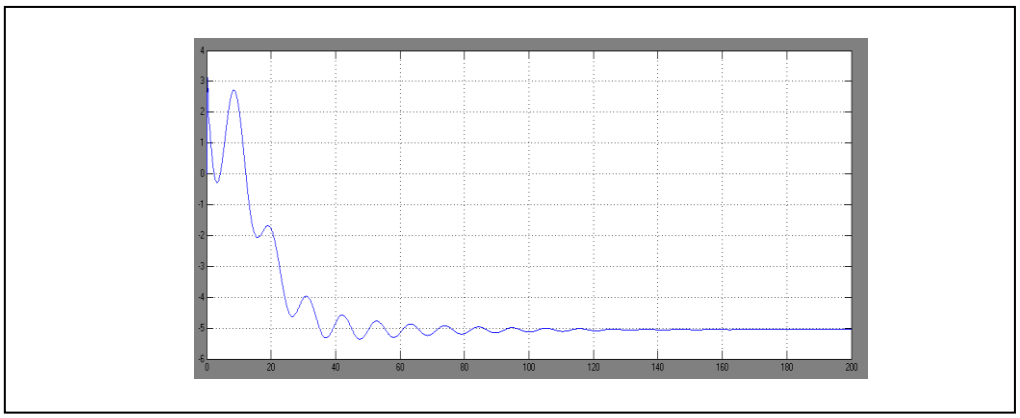

Fig. 18: Pitch Angle open-loop response (spiral mode).

The lateral controller was first designed to stabilise the lateral dynamics of the UAV. This was followed by the longitudinal controller to control the pitch angle. The overall design was then adapted to perform servoing using the information from the VBN sensors and integrated VIG/VIG/GAD navigation systems. The lateral and longitudinal controllers were implemented on Matlab using the Fuzzy Logic Toolbox. The Mamdani fuzzy inference system (FIS) from the toolbox was used to create the membership functions. Based on the input and output membership functions, the fuzzy rules were developed that relate the inputs and the output. The membership functions and the rules were modified by trial and error to obtain better responses. Triangular and trapezoidal membership functions were used for the membership functions due to their simplicity and ease of implementation. A rough estimate of the membership functions was used for all the variables which were then modified as required. The membership functions which gave the best results for the roll and pitch responses were selected. Linguistic variables were used to define the fuzzy sets of inputs and the outputs of the controller. The fuzzy sets and the range of the inputs and outputs are shown in Tables 4 and 5, where VN = Very Negative, VP = Very Positive, VH = Very High, VL = Very Low, SN = Slightly Negative, SP = Slightly Positive, SH = Slightly High, SL = Slightly Low, Z = Zero

.

Table 4: Fuzzy sets and range of inputs.

Input Variable	Fuzzy Set	Range
Roll Error	VN, SN, Z, SP, VP	-180° to 180°
Roll Rate	VN, SN, Z, SP, VP	-40°/s to 40°/s
Pitch Error	VL, SL, Z, SH, VH	-90° to 90°
Deviation	VN, SN, Z, SP, VP	-512 pixels to 512 pixels

Deviation Rate	VN, SN, Z, SP, VP	-600 pixels/s to 600 pixels/s

Table 5: Fuzzy sets and range of outputs.

Output Variable	Fuzzy Set	Range
Aileron Deflection	VN, SN, Z, SP, VP	-60° to 60°
Elevator Deflection	VN, SN, Z, SP, VP	-60° to 60°
Required Roll to correct Deviation	VN, SN, Z, SP, VP	-60° to 60°

The lateral controller design was designed with the aim of stabilising the roll of the aircraft during the landing phase. This was required to maintain zero roll during touchdown at the centre of the runway so as to avoid wing-strike on the runway. It also controlled the position of the aircraft with respect to the centreline of the runway. Inputs to the controller were the Roll Error, Roll Rate, Deviation and the Deviation Rate and the output was the Aileron Deflection in degrees. The difference between the current roll angle given by the AEROSONDE model with the required value was used to represent the Roll Error. A gain of (π/180) was applied to the Aileron Deflection to convert it into radians. The flap and elevator deflection were set to zero while the throttle was set to full (one). The mixture, ignition and wind were kept at their default settings. The system was simulated for 200 iterations on Simulink with a required roll of 0°. Various membership functions of the Roll Error and Aileron Deflections were considered in order to identify the most optimal FLC for stabilization. The simulation was then repeated with a required roll of 15°. The fuzzy rules used are as follows:

- If (Roll is Z) then (Aileron_Deflection is Z)
- If (Roll is SP) then (Aileron_Deflection is SP)
- If (Roll is SN) then (Aileron_Deflection is SN)
- If (Roll is VN) then (Aileron_Deflection is VN)
- If (Roll is VP) then (Aileron_Deflection is VP)

The Roll Rate was added to the controller so as to give it a higher degree of control. The membership functions for the Roll Rates were developed using the same methodology used for Roll Error and Aileron Deflection. 25 fuzzy rules were developed for the FLC and their surface representation is given in Fig. 19.

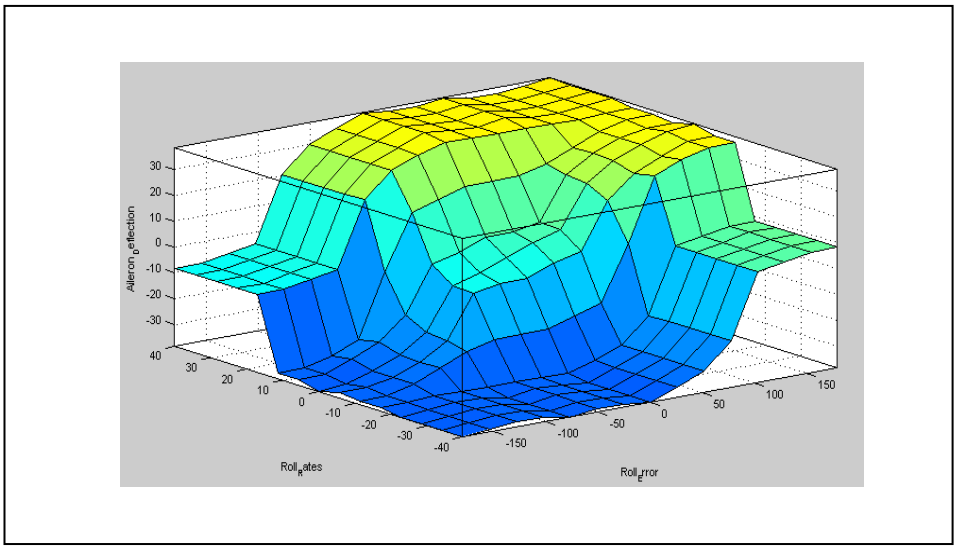

Figure 19: Fuzzy rules for roll control.

A steady-state error and overshoot were observed from the roll response of the aircraft. Therefore, a PID controller was desgined to eliminate these errors. PID tuning was carried out to find the values for the gains which gave the optimal roll response. The deviation from the centerline of the runway was controlled using the roll of the aircraft. The value of the Deviation and Deviation Rate was used by the controller to calculate

the Required Roll. A surface representation of the fuzzy rules is given in Fig. 20.

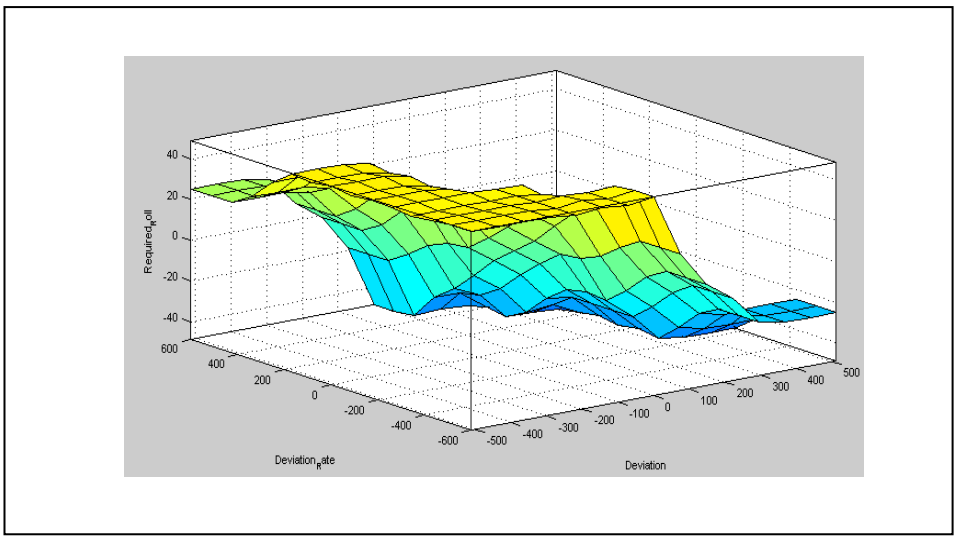

Figure 20: Fuzzy rules for deviation control.

The longitudinal controller was used to stabilise and control the Pitch of the aircraft using Elevator Deflections. Prior to design, it was observed that the pitch angle was stabilised to some extent due to the lateral controller as shown in Fig. 21.

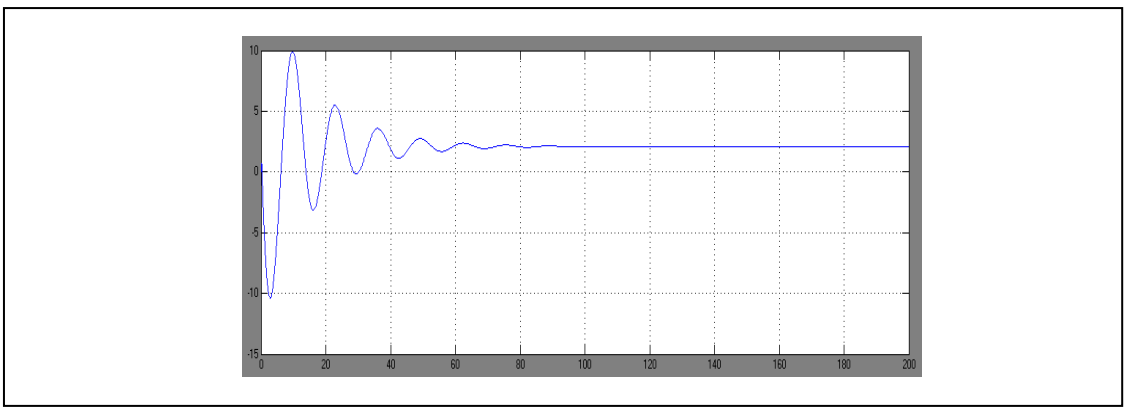

Figure 21. Partially stabilised pitch response due to lateral controller.

The design process of the longitudinal controller followed the same methodology as that of the lateral controller. The FLC was first designed using trial-and-error for the membership functions of Pitch Error and Elevator Deflections followed by the PID controller. A derivative gain was used instead of pitch rates. The fuzzy rules used for the longitudinal controller are given below:

- If (Pitch is Z) then (Elevator_Deflection is Z)
- If (Pitch is SH) then (Elevator_Deflection is SP)
- If (Pitch is SL) then (Elevator_Deflection is SN)
- If (Pitch is VH) then (Elevator_Deflection is VN)
- If (Pitch is VL) then (Elevator_Deflection is VP)

The overall architecture of the controller (lateral and longitudinal components) is shown in Fig. 22.

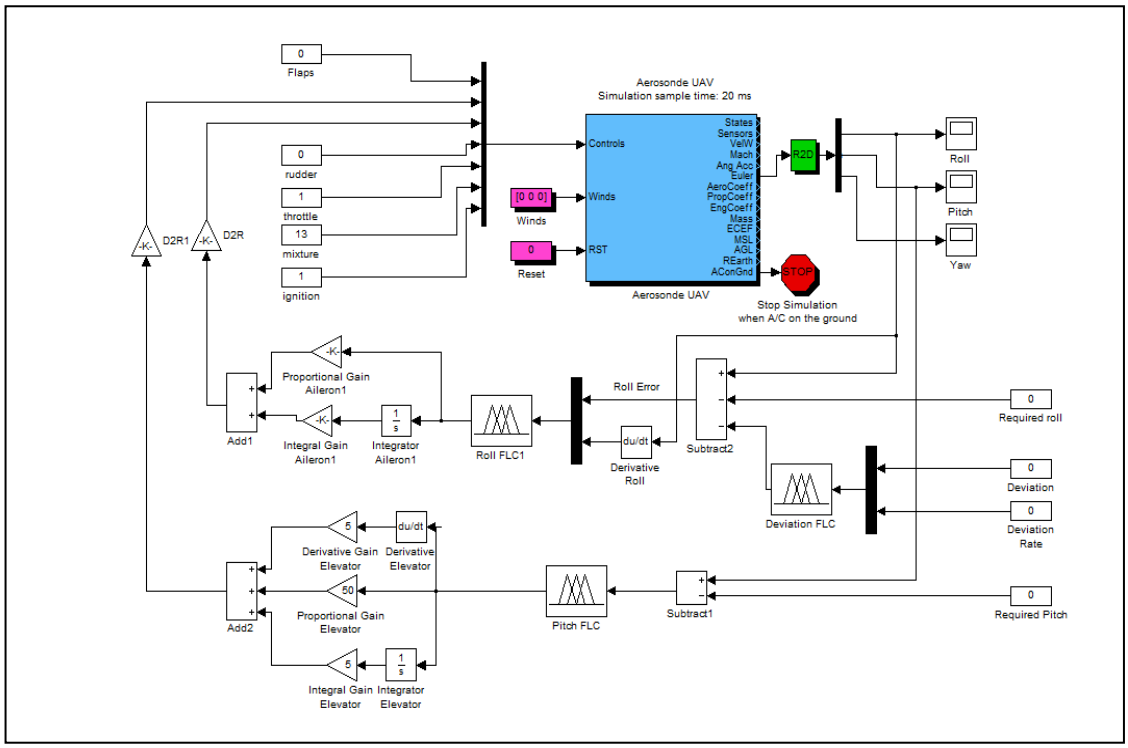

Figure 22. Overall design of the controller.

The pitch and roll responses of the controller are shown in Fig. 23 and Fig. 24.

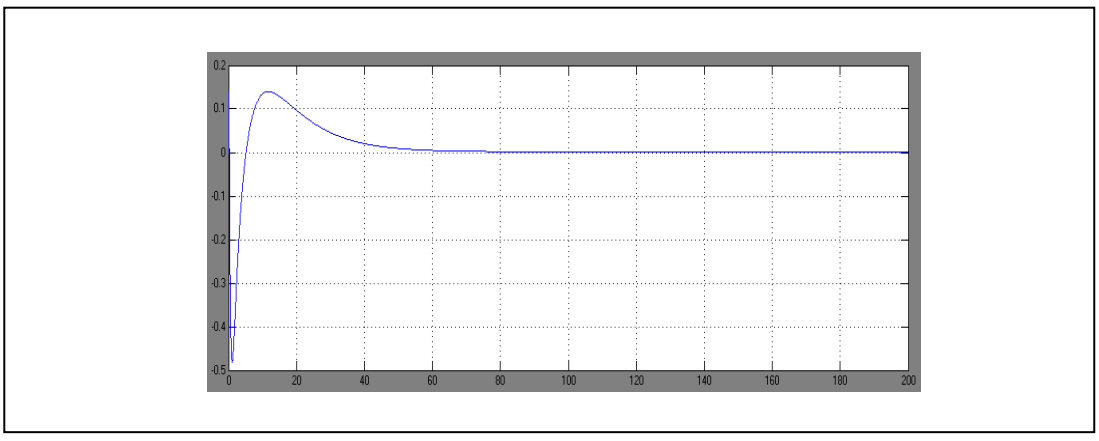

Figure 23. Pitch response with controller.

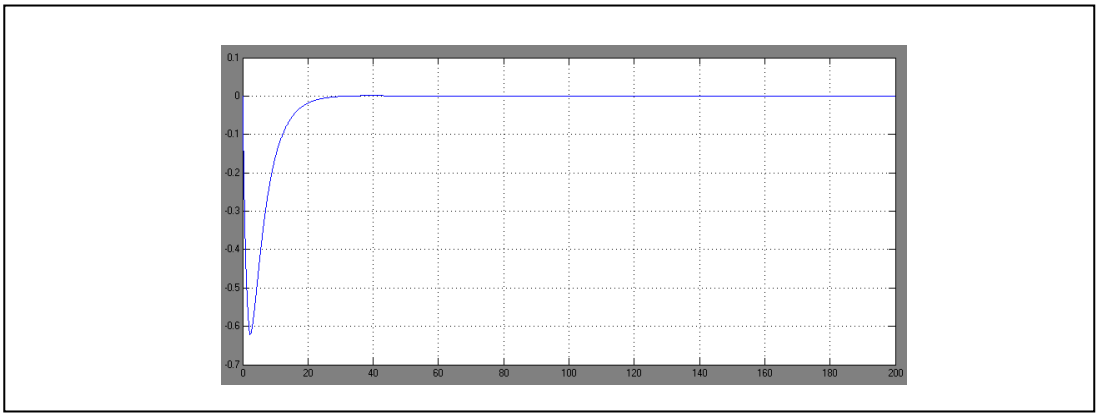

Figure 24. ϕ (roll) response with controller.

The results show that the pitch and roll converge rapidly towards the required value of zero after a short initial instability. Comparing these results with the uncontrolled response in Fig 17 and Fig. 18, we can confirm that the controller gives satisfactory results. The simulation showed that the controller is able to correct the attitude disturbances caused by moderate to high wind speeds. However, it was observed that the aircraft became unstable with lateral wind speeds exceeding 20 m/s.

5. VIG AND VIG/GAD SIMULATION

In order to evaluate the performance of the integrated VIG/GAD system in conjunction with the Fuzzy/PID controller, a simulation was carried out using the AEROSONDE UAV platform. A suitable flight profile was defined including a number of representative flight manoeuvres [15]. The duration of the simulation is 1150 seconds. The horizontal and vertical flight profiles are shown in Fig. 25.

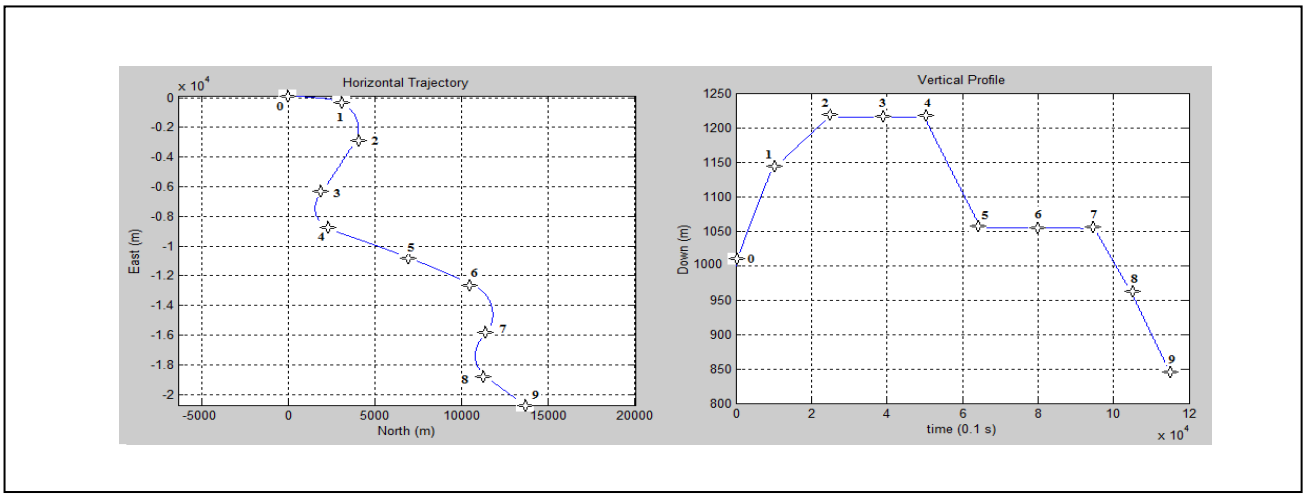

Figure 25. Horizontal and vertical flight profiles.

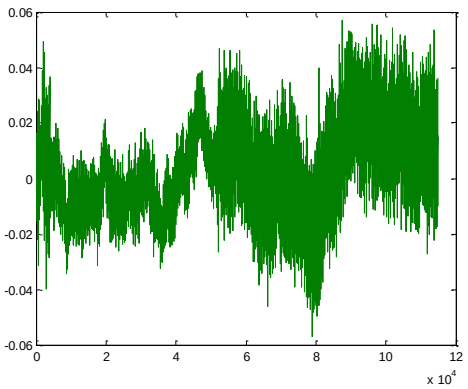

VIG system

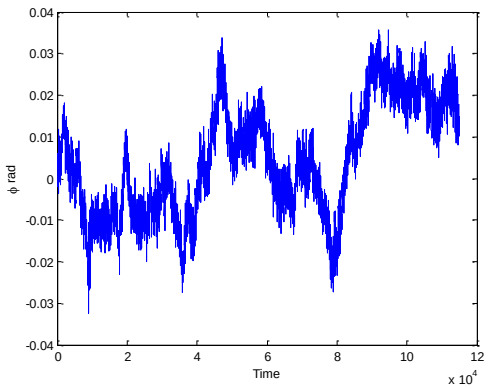

VIG + GAD with 3 antennae

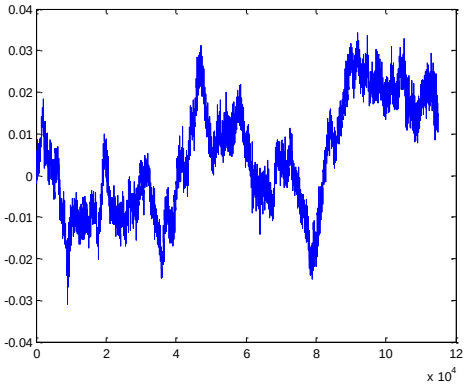

VIG + GAD with 4 antennae

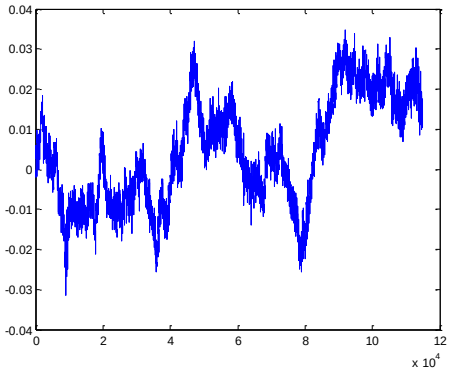

VIG + GAD with 5 antennae

Figure 26. Roll (ϕ) error time histories.

Fig. 26 shows a graphical comparison of the ϕ (roll) error obtained with the VIG and the VIG/GAD systems. It is observed that the VIG/GAD system, with 3, 4 and 5 antennae provides a significant improvement over the VIG system. Table 6 provides the roll error mean and standard deviation values. The performance achieved with 4 and 5 antennae is similar.

Table 6: Roll (ϕ) error statistics (degrees).

Phases of Flight	VIG		VIG/GAD 3 Antennae		VIG/GAD 4 Antennae		VIG/GAD 5 Antennae	
	Mean	σ	Mean	σ	Mean	σ	Mean	σ
Straight Climb	2.13E-01	3.04E-01	2.23E-01	1.66E-01	2.19E-01	1.24E-01	2.20E-01	1.35E-01
Right Turn Climb	5.47E-01	3.41E-01	5.55E-01	1.88E-01	5.56E-01	1.85E-01	5.55E-01	1.85E-01
Straight and Level	2.32E-01	3.73E-01	2.53E-01	2.01E-01	2.52E-01	1.49E-01	2.52E-01	1.63E-01
Level Left Turn	1.12E-01	2.04E-01	1.27E-01	1.61E-01	1.19E-01	1.34E-01	1.21E-01	1.39E-01
Straight Descent	1.07E-01	2.57E-01	9.03E-02	2.05E-01	9.57E-02	1.78E-01	9.32E-02	1.83E-01
Level Right Turn	-8.86E-01	2.81E-01	-9.18E-01	2.69E-01	-9.23E-01	2.42E-01	-9.21E-01	2.48E-01
Left Turn Descent	-5.71E-01	1.98E-01	-6.12E-01	1.48E-01	-6.11E-01	1.33E-01	-6.11E-01	1.34E-01

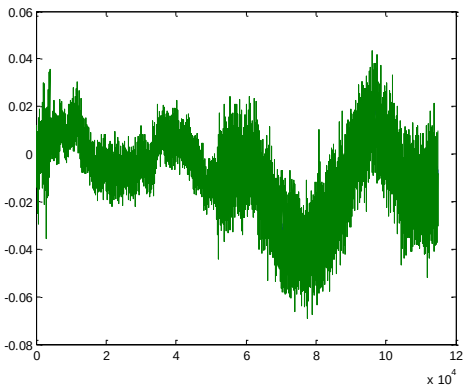

VIG system

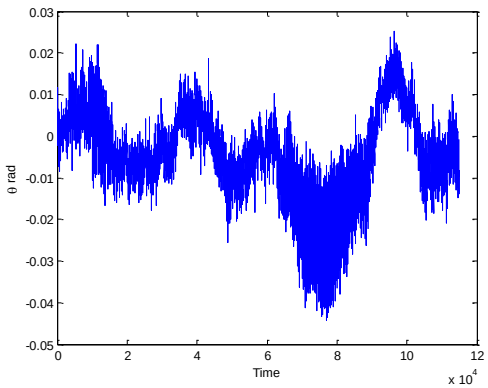

VIG + GAD with 3 antennae

ARPN Journal of Systems and Software

http://www.scientific-journals.org

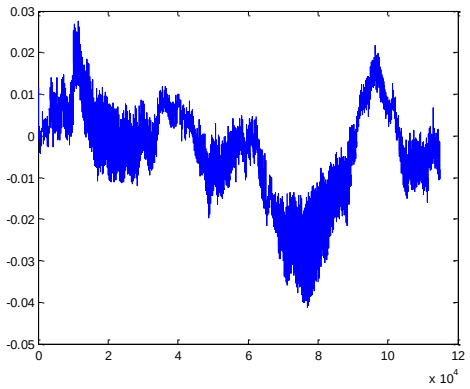

VIG + GAD with 4 antennae

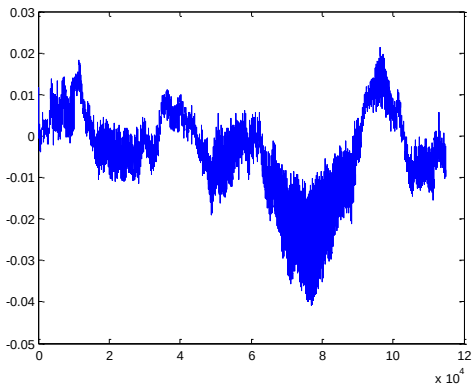

VIG + GAD with 5 antennae

Figure 27: θ (pitch) angle error time histories.

Fig. 28 presents a similar comparison for the θ (pitch) angle. There is a significant improvement with the GAD integration. In this case it is also observed that the error decreases significantly when the number of antennae is increased. Table 7 confirms such improvement by showing the values of means and standard deviation for different phases of flight.

Table 7: Pitch (θ) error statistics (degrees).

Phases of Flight	VIG		VIG/GAD 3 Antennae		VIG/GAD 4 Antennae		VIG/GAD 5 Antennae	
	Mean	σ	Mean	σ	Mean	σ	Mean	σ
Straight Climb	-6.17E-02	2.25E-01	-1.27E-02	1.81E-01	-2.81E-02	1.09E-01	-2.32E-02	1.07E-01
Right Turn Climb	1.45E-01	2.23E-01	1.28E-01	1.24E-01	1.22E-01	7.84E-02	1.27E-01	7.34E-02
Straight and Level	3.15E-01	3.67E-01	2.89E-01	2.78E-01	2.85E-01	2.41E-01	2.89E-01	2.40E-01
Level Left Turn	4.74E-01	1.27E-01	4.21E-01	1.86E-01	4.06E-01	1.02E-01	4.06E-01	9.67E-02
Straight Descent	4.17E-01	1.55E-01	3.44E-01	2.21E-01	3.47E-01	1.21E-01	3.50E-01	1.12E-01
Level Right Turn	4.26E-01	1.43E-01	3.73E-01	2.16E-01	3.60E-01	1.19E-01	3.63E-01	1.09E-01
Left Turn Descent	6.48E-01	1.40E-01	5.03E-01	2.57E-01	6.62E-01	1.89E-01	5.96E-01	1.15E-01

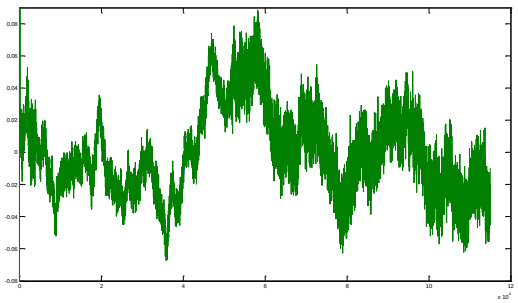

VIG system

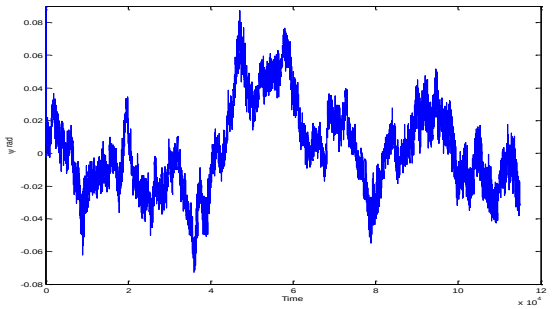

VIG + GAD with 3 antennae

ARPN Journal of Systems and Software

http://www.scientific-journals.org

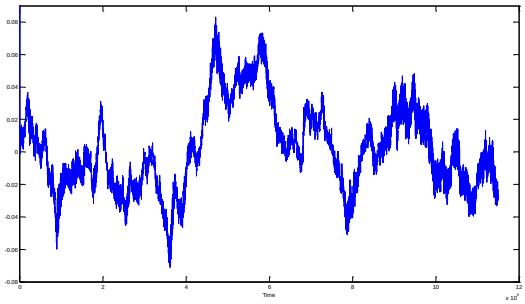

VIG + GAD with 4 antennae

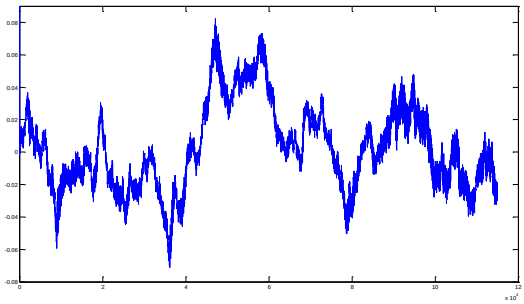

VIG + GAD with 5 antennae

Figure 28: Yaw (ψ) error time histories.

Finally in Fig. 29 a similar behaviour is observed for the yaw error. The tendency to improvement versus the VIG system is observed for all phases of flight. Table 8 provides the mean and standard deviation values.

Table 8: Yaw (ψ) error statistics (degrees).

Phases of Flight	VIG		VIG/GAD 3 Antennae		VIG/GAD 4 Antennae		VIG/GAD 5 Antennae	
	Mean	Σ	Mean	σ	Mean	σ	Mean	σ
Straight Climb	-7.63E-01	2.21E-01	-1.01	2.17E-01	-8.35E-01	2.16E-01	-8.52E-01	2.05E-01
Right Turn Climb	1.08	4.24E-01	1.15	3.79E-01	1.14	3.71E-01	1.14	3.71E-01
Straight and Level	4.74E-01	3.67E-01	5.40E-01	3.93E-01	5.40E-01	3.07E-01	5.40E-01	2.93E-01
Level Left Turn	2.35E-01	2.87E-01	2.94E-01	3.06E-01	2.79E-01	2.60E-01	2.76E-01	2.58E-01
Straight Descent	2.26E-01	3.79E-01	2.09E-01	3.94E-01	2.18E-01	3.46E-01	2.20E-01	3.42E-01
Level Right Turn	-1.74	5.74E-01	-1.84	5.40E-01	-1.85	4.95E-01	-8.18E-01	4.90E-01
Left Turn Descent	-1.07	3.95E-01	-1.22	3.32E-01	-1.21	3.15E-01	-1.21	3.18E-01

For completeness, the accuracies in roll, pitch and roll obtained with the standalone GAD system with combinations of 3, 4 and 5 antennae are shown in Tables 9, 10 and 11. Using three antennae, the standalone GAD system exhibit lower standard deviation values than the VIG system for climb and level flight (similar performances are achieved in the other flight phases). As expected, when the number of antennae increases the error of the GAD system decreases.

Table 9: Stand-alone GAD roll (ϕ) error statistics (degrees).

Phases of Flight	3 Antennae		4 Antennae		5 Antennae	
	Mean	Σ	Mean	σ	Mean	σ
Straight Climb	2.22E-01	1.80E-01	2.16E-01	1.29E-01	2.18E-01	1.43E-01
Right Turning Climb	5.59E-01	1.91E-01	5.61E-01	1.86E-01	5.61E-01	1.86E-01
Straight and Level	2.59E-01	2.16E-01	2.59E-01	1.54E-01	2.59E-01	1.72E-01
Level Left Turn	1.31E-01	1.68E-01	1.20E-01	1.36E-01	1.23E-01	1.41E-01
Straight Descent	8.47E-02	2.12E-01	9.14E-02	1.81E-01	8.91E-02	1.86E-01
Level Right Turn	-9.38E-01	2.80E-01	-9.44E-01	2.47E-01	-9.42E-01	2.54E-01
Left Turning Descent	-6.34E-01	1.60E-01	-6.34E-01	1.44E-01	-6.34E-01	1.44E-01

Table 10: Stand-alone GAD pitch (θ) error statistics (degrees).

Phases of Flight	3 Antennae		4 Antennae		5 Antennae	
	Mean	Σ	Mean	σ	Mean	σ
Straight Climb	5.60E-03	2.00E-01	-1.65E-02	1.18E-01	-8.30E-03	1.15E-01
Right Turning Climb	1.19E-01	1.35E-01	1.09E-01	8.22E-02	1.16E-01	7.60E-02
Straight and Level	2.68E-01	2.79E-01	2.63E-01	2.32E-01	2.70E-01	2.30E-01
Level Left Turn	3.82E-01	2.01E-01	3.62E-01	1.16E-01	3.62E-01	1.09E-01
Straight Descent	3.05E-01	2.41E-01	3.08E-01	1.29E-01	3.12E-01	1.20E-01
Level Right Turn	3.37E-01	2.39E-01	3.21E-01	1.30E-01	3.25E-01	1.19E-01
Left Turning Descent	4.19E-01	2.98E-01	6.74E-01	2.46E-01	5.68E-01	1.33E-01

Table 11: Stand-alone GAD yaw (ψ) error statistics (degrees).

Phases of Flight	3 Antennae		4 Antennae		5 Antennae	
	Mean	Σ	Mean	σ	Mean	σ
Straight Climb	-9.42E-01	2.92E-01	-9.13E-01	2.19E-01	-9.01E-01	2.07E-01
Right Turning Climb	1.18	3.88E-01	1.18	3.76E-01	1.18	3.76E-01
Straight and Level	5.77E-01	4.20E-01	5.76E-01	3.18E-01	5.76E-01	3.01E-01
Level Left Turn	3.19E-01	3.13E-01	3.01E-01	2.56E-01	2.98E-01	2.53E-01
Straight Descent	2.06E-01	4.02E-01	2.17E-01	3.42E-01	2.19E-01	3.38E-01
Level Right Turn	-1.90	5.64E-01	-1.91	5.10E-01	-1.92	5.04E-01
Left Turning Descent	-1.31	3.51E-01	-1.30	3.33E-01	-1.30	3.36E-01

6. CONCLUSIONS

In this paper we have investigated the potential of GAD systems for integration in small size UAVs. Processing algorithms have been proposed, which allow a fast and reliable computation of the vehicle attitude data. A recursive algorithm has been proposed for combining multiple attitude measurements obtained from different antenna locations, and its efficiency has been analysed in various dynamic conditions using the AEROSONDE UAV platform as a representative test case. Modelling and simulation activities also considered the possible augmentation provided by GAD to a low-cost and low-weight/volume VIG integrated navigation system employing a VBN, MEMS-IMU and code-range GNSS (i.e., GPS and GALILEO) for position and velocity computations. Integration of the GAD with the VIG system using an EKF was accomplished. Considering the AEROSONDE UAV and a number of possible GNSS antenna network configurations, it was demonstrated that, in a variety of dynamics conditions, the accuracy of the VIG/GAD attitude solution was comparable to the accuracy obtainable with traditional inertial sensors. However, the accuracy could be significantly influenced by the chosen antenna network geometry and the number of antennae available. Compared to the VIG system, the VIG/GAD shows an improvement of the accuracy in all three attitude angles. The magnitude of this improvement varies for each angle and for different flight phases. As expected, as the number of antennae increases, also the accuracy improves. The design of the Fuzzy/PID controller was successfully accomplished. However, during the test activities, it was observed that the Fuzzy/PID controller becames unstable at wind speeds greater than 20 m/s. In case of pure visual servoing during the approach and landing phase, this would lead to the impossibility of tracking the desired features from the surrounding. Current research activities at Cranfield University are investigating the potential of low-cost GNSS attitude sensors (two or more antennae) in various classes of UAVs and Unmanned Space Vehicles (USVs). Additionally, multipath and shielding problems are being carefully modelled and adequate algorithms are being developed in order to cope with these effects during high dynamics manoeuvres.

7. REFERENCES

[1] Gebre-Egziabher, D., Hayward R. and Powell. J, “A Low-Cost GPS/Inertial Attitude Heading Reference System (AHRS) for General

Aviation Applications." 1998 IEEE Position, Location and Navigation Symposium - PLANS '98, Palm Springs, California. 1998.

[2] Angrisano, A., "GNSS/INS integration methods." Dottorato di ricerca (PhD) in Scienze Geodetiche e Topografiche Thesis, Universita' degli Studi di Napoli "PARTHENOPE", Naple. 2010

[3] Nassar, S., "Improving the Inertial Navigation System (INS) Error Model for INS and INS/DGPS Applications." UCGE Reports Number 20183, University of Calgary, Department of Geomatics Engineering, Alberta, Canada. 2003.

[4] Godha, S., "Performance Evaluation of Low Cost MEMS-Based IMU Integrated With GPS for Land Vehicle Navigation Application." UCGE Report No. 20239, University of Calgary, Department of Geomatics Engineering, Alberta, Canada. 2006.

[5] Molina, P., Wis, M., Pares, M.E., Blazquez, M., Tatjer, J.C., Colomina, I., "New Approaches to IMU Modeling and INS/GPS Integration for UAV-Based Earth-Observation." *Proceedings of the 21st International Technical Meeting of the Satellite Division of The Institute of Navigation*, Savannah, GA, September 2008, pp. 1335-1344. 2008.

[6] Cohen, C., et al., "Flight Tests of Attitude Determination Using GPS Compared Against an Inertial Navigation Unit." Navigation (ION Journal), Vol. 41. 1994.

[7] Van Grass, F., et al., "GPS Interferometric Attitude and Heading Determination: "Initial Flight Test Results", Navigation (ION Journal), Vol. 38. 1991.

[8] Brown, A.K., et al., "Interferometric Attitude Determination Using GPS." Proceedings of the Third International Geodetic Symposium on Satellite Doppler Positioning, Las Cruces, NM. Vol II. pp 1289-1304. 1982.

[9] Giorgi, G.; Teunissen, P. J. G.; Gourlay, T. P., "Instantaneous Global Navigation Satellite System (GNSS)-Based Attitude Determination for Maritime Applications." *Oceanic Engineering, IEEE Journal of* , vol.PP, no.99. 1996

[10] Pinchin, J., "GNSS Based Attitude for Small Unmanned Aerial Vehicle." PhD Thesis, University of Cantenbury, 2011.

[11] Keong, J., "Determining Heading and Pitch Using a Single Difference GPS/GLONASS Approach." PhD Thesis, Department of Geomatics Engineering, University of Calgary. 2007.

[12] Giorgi, G., Teunissen, P.J.G., "Carrier phase GNSS attitude determination with the Multivariate Constrained LAMBDA method." *Aerospace Conference, 2010 IEEE* , vol., no., pp.1-12, 6-13. 2010

[13] P. J. G. Teunissen, "The Least-Squares Ambiguity Decorrelation Adjustment: a Method for Fast GPS Integer Ambiguity Estimation." Journal of Geodesy, Vol. 70, pp. 65–82. 1995.

[14] Sabatini, R., Kaharkar, A., Shaid, T., Bartel, C., Jia, H., Zammit-Mangion, D., "Vision-based Sensors and Integrated Systems for Unmanned Aerial Vehicles Navigation and Guidance." Proceedings of the SPIE Conference Photonics Europe 2012. Brussels (Beligium). 2012.

[15] Sabatini, R., Kaharkar, A., Shaid, T., Bartel, C., Jia, H., Zammit-Mangion, D., "Low-cost Vision Sensors and Multisensor Systems for Small to Medium Size UAV Navigation and Guidance." Proceedings of the European Navigation Conference 2012. Gdansk (Poland). 2012.

[16] Cohen, C. E., "Attitude Determination Using GPS." PhD Thesis, Stanford University. 1992.

[17] Saripalli, S., Montgomery, J.F. and Sukhatme, G.S., "Vision Based Autonomous Landing of an Unmanned Aerial Vehicle." Proceedings of International Conference of Robotics and Automation, ICRA2002, Washington DC, Virginia, USA. 2002.

[18] Gong, X., Abbott, A.L. and Fleming, G.A., "A Survey of Techniques for Detection and Tracking of Airport Runways." Collection of Technical Papers, 44th AIAA Aerospace Sciences Meeting and Exhibit, pp. 1-14, vol. 23. 2006.

[19] Chen, Z. and Birchfield, S.T., "Qualitative vision-based path following." IEEE Trans. on Robotics, Vol. 25, Issue 3, pp. 749-754. 2009.

[20] Nixon, M.S. and Aguado, A.S., "Feature Extraction and Image Processing." Newnes, 1st Edition. 2002.

[21] Sangyam, T., Laohapiengsak, P., Chongcharoen, W. and Nilkhamhang, I., "Path tracking of UAV using self-tuning PID controller based on Fuzzy Logic." Proceedings of SICE Annual Conference, pp. 1265-1269. 2010.

[22] B. W. Parkinson, "GPS error analysis." Global Positioning System: Theory and Applications, AIAA, vol. pp. 469-483. 1996.

[23] Hopfield, H. S., "Tropospheric effect on electromagnetically measured range: Prediction from surface weather data." In *Radio Science*, 6(3): 357 – 367. 1971.

[24] McGraw, G.A., "Tropospheric Error Modeling for High Integrity Airborne GNSS Navigation." IEEE/ION Position Location and Navigation Symposium. 2012.

[25] Kleijer, F., "Troposphere Modeling and Filtering for Precise GPS Leveling." Nederlandse Commissie voor Geodesie (Netherlands Geodetic Commission). 2004.

[26] Lau, L., Cross, P., "A New Signal-to-Noise-Ratio Based Stochastic Model for GNSS High-Precision Carrier Phase Data Processing Algorithms in the Presence of Multipath Errors." Proceedings of the 19th International Technical Meeting of the Satellite Division of the Institute of Navigation, Fort Worth, TX, pp. 276-285. 2006,

[27] Brunner, F., et al., "GPS Signal Diffraction Modelling: the Stochastic SIGMA-D Model", Journal of Geodesy, 73(5), pp 259–267. 1999.

[28] Wieser, A., et al., , Improved Positioning Accuracy with High Sensitivity GNSS Receivers and SNR Aided Integrity Monitoring of Pseudo-range Observations." Proceedings of the 18th International Technical Meeting of the Satellite Division of Institute of Navigation, Long Beach, CA, pp. 13–16. 2005.

[29] Misra, P, Enge, P., "Global Positioning System: Signal, Measurements, and Performance." Ganga-Jamuna Press, USA. 2001.

[30] Park, C., Kim, I., "An Error Analysis of 2-Dimensional Attitude Determination System Using Global Positioning System." IEEE Transactions on Communications, Vol. E83-B, No. 6, pp. 1370-1373. 2000.

[31] Park, C., et al., "Error Analysis of 3-Dimensional GPS Attitude Determination System", International Journal of Control, Automation, and Systems, Vol. 4, No. 4, pp. 480-485. 2006.

[32] Unmanned Dynamics LLC, "AeroSym Aeronatical Simulation Blockset User's Manal." Available online at: http://people.rit.edu/pnveme/EMEM682n/Matlab_682/aerosim_ug.pdf (website visited in 2012).

[33] Maurer, J., "Polar Remote Sensing Using an Unpiloted Aerial Vehicle (UAV)." Seminar by Dr. James Maslanik, Colorado Center for Astrodynamics Research (CCAR), University of Colorado at Boulder. Available online at: http://www2.hawaii.edu/~jmaurer/uav/#specifications (website visited in 2012).